ASI & CAIF Summer Internship Final Report
Low Energy tour of the Galilean moons

Andrea Viale
MSc student at
University of Padua, Italy
Visiting scholar at
Purdue University, IN

October 25, 2016

1 Acknowledgements

I would like to thank Prof. Kathleen C. Howell for accepting me in her prestigious research group in multi-body dynamics at Purdue University, department of Aeronautics and Astronautics. A special thank goes to Prof. Giorgio Bellettini and Prof. Simone Donati for their help and support with the bureaucratic procedures. Finally, I want to show my appreciation to ASI (Italian Space Agency) and CAIF (Cultural Association of Italians at Fermilab) for this important opportunity they offered and the internship grant.

2 Introduction

The present report partially summarizes the work done during my internship at Purdue University. The study is within the field of the astrodynamics, and deals with efficient design of low-energy transfers in planetary system. Motivated by the growing interest in the robotic exploration of the Jovian system, which has given rise to numerous studies and mission proposals, we apply the method to three Galilean moons orbiting around Jupiter. The first chapter is an introduction to the circular restricted three body problem, which is the framework of the work. The second chapter briefly summarize the method used with an application to a two-moons coupling. Eventually, results for the three-moon coupling are presented.

3 The circular restricted three-body problem

Studying the dynamics of n bodies subjected to their mutual gravitational attraction is the main purpose of orbital mechanics. The so called *two-body prob-*

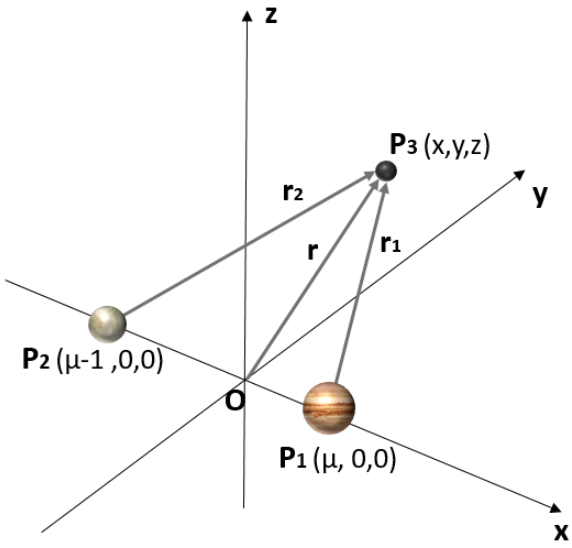

Figure 1: The synodical reference frame. With the convention used in this work P_1, i.e., the heavier body, has positive x coordinate. r_i $(i = 1, 2)$ is the position vector connecting P_i with P_3, while $r = (x, y, z)$ is the position vector connecting the origin O with P_3.

lem, corresponding to $n = 2$, was first studied and solved by Johann Bernoulli (1667-1748). This problem considers two masses (for example a spacecraft and the Earth) approximated as points and acted upon only by the mutual force between them. The solution to this problem is analytical and shows that the two bodies revolve around their mutual barycentre describing an elliptical motion. In real cases, however, considering more than two bodies may provide more accurate solutions. With the *three-body problem*, for instance, to motion of a point mass P_3 with respect to two other masses P_1 and P_2 is considered. If P_3 is vanishingly small with respect to the other two masses we talk about the *restricted three body problem*. Eventually, if the motion of P_1 and P_2 is assumed to by circular (and centred on their barycentre) we are referring to the *circular restricted three body problem* (CR3BP)[1]. The main elements of the CR3BP are here briefly introduce; fundamental references include [1, 2, 3, 4, 5] for the CR3BP and [6, 7, 8] for the dynamical systems theory.

Let the synodical reference frame (SRF) be the co-moving frame whose x-axis always contain the two primaries P_1 and P_2 in fixed positions, with the origin on their barycentre. The SRF rotates with constant angular velocity $\omega = 2\pi/T$ with respect to an inertial reference frame centred on O, being T the

period of the primaries. Moreover, we define the *mass ratio* of the system as:

$$\mu = \frac{m_2}{m_1 + m_2}, \tag{1}$$

being m_i the mass of P_i $(i = 1, 2)$. Introducing a set of nondimensional coordinates such that the distance between P_1 and P_2, the sum of their masses and the angular velocity are unitary quantities, the equations of motion of P_3 in the SRF are a solely function of the mass ratio:

$$\ddot{x} = 2\dot{y} + x - \frac{(1-\mu)(x-\mu)}{r_1^3} - \frac{\mu(x+1-\mu)}{r_2^3} \tag{2a}$$

$$\ddot{y} = y - 2\dot{x} - \frac{(1-\mu)y}{r_1^3} - \frac{\mu y}{r_2^3} \tag{2b}$$

$$\ddot{z} = -\frac{(1-\mu)z}{r_1^3} - \frac{\mu z}{r_2^3} \tag{2c}$$

where r_i $(i = 1, 2)$ is the position vector connecting P_i with P_3. Furthermore, these equations are autonomous, since there is not explicit dependence on time. They are also nonlinear because of the dependence from the inverse of the third power of the distances r_1 and r_2. Eventually, Eqs. (2) admit a first integral J, called *Jacobi constant*:

$$J = x^2 + y^2 + \frac{2(1-\mu)}{r_1} + \frac{2\mu}{r_2} + [\mu(1-\mu)] - (\dot{x} + \dot{y}^2 + \dot{z^2}). \tag{3}$$

Its values is linked to the mechanical energy of the system E, being $E = -J/2$.

The term $\dot{x} + \dot{y}^2 + \dot{z}^2$ on the right-hand side of Eq. (3) is the magnitude of the velocity squared. Rearranging Eq. (3) with $\dot{x} + \dot{y}^2 + \dot{z}^2 = 0$ permits to define three-dimensional zero-velocity surfaces (ZVSs), known as *forbidden regions*, which separate regions where the motion of P_3 is permitted from regions where it is not allowed (since the magnitude of the velocity squared would be negative). A projection of these surfaces onto the xy plane results in the so called zero-velocity curves (ZVCs). The region surrounding the larger primary is often defined as *interior* region, the region in the vicinity of the smaller primary as P_2 region and the region beyond the ZVCs as *exterior* region. An example of these surfaces is provided in Fig. 2.

3.1 Equilibrium points

In the SRF it is possible to identify specific points, the *equilibrium points*, in which the combined gravitational pull exerted by P_1 and P_2 on P_3 is exactly balanced by the centripetal force required by P_3 to rotate with the SRF itself. These positions can be found by imposing

$$\dot{x} = \dot{y} = \dot{z} = 0; \quad \ddot{x} = \ddot{y} = \ddot{z} = 0 \tag{4}$$

in Eqs. (2). Therefore if P_3 is placed in one of these points with zero velocity and acceleration it will remain still with respect to the SRF (therefore moving in

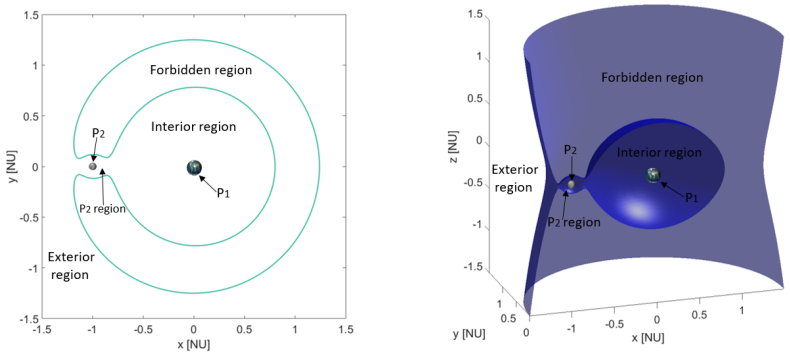

(a) Zero velocity curves (b) Zero velocity surfaces

Figure 2: ZVCs and ZVSs (a three-dimensional cut on a x-z plane is displayed) for the Earth-Moon system with $J = 3.17$ (Earth and Moon are not to scale). At this energy level, P_3 is allowed to move inside the whole realm of interior region, P_2 region and exterior region. [NU] in the axes stands for *nondimensional units*

circular motion with respect to the IRF). Comparing Eq. (4) with (2c) it follows that the equilibrium points lie in the orbital plane of the primaries. Combining Eqs. (2a),(2b) with (4) it can be shown that five equilibrium points exist and these are classified into two categories [1].

- Collinear equilibrium points (also known as *libration* or *Lagrangian* points). They lie on the x-axis and they are called L_1, L_2, L_3.
- Triangular equilibrium points. They lie at the vertexes of two equilateral triangles, whit unitary side (in nondimensional units).

Their positions for the Earth-Moon CR3BP are shown is Fig. 3.

Studying the stability of the equilibrium points is fundamental to exploit the dynamics of the CR3BP. The equations of motion (2) in the neighbourhood of these points can be linearised in the form:

$$\dot{\mathbf{x}} = \mathbf{A}\mathbf{x}. \tag{5}$$

where $\mathbf{A}$ is a constant matrix, whose elements vary according to the equilibrium point considered. It can be shown that:

- the collinear equilibrium points behave linearly as the product of two centres by a saddle, i.e., in their vicinity there exist bounded orbits (associated with the central part) and escape trajectories (associated with the saddle part);
- the triangular equilibrium points are unstable when the mass ratio $\mu < \mu_{\text{critic}} = 1/2(1 - \sqrt{69}/9) \approx 0.038521$.

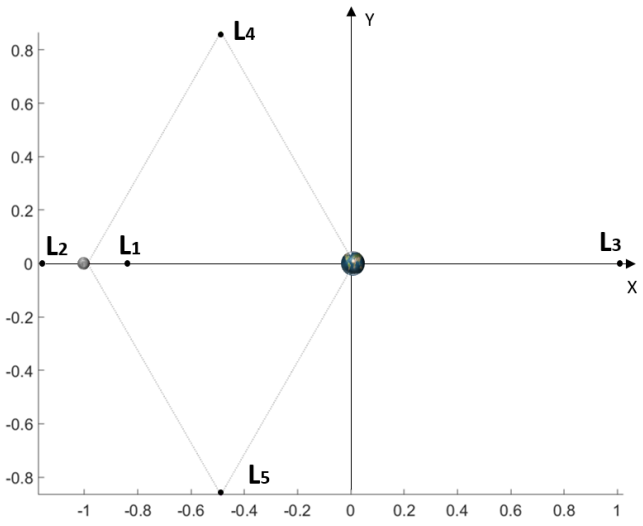

Figure 3: Positions of the equilibrium points for the Earth-Moon CR3BP ($\mu = 0.121506683 \times 10^{-1}$).

The value of μ_{critic} is rather high: for instance, the mass ratio of the CR3BPs composed by the Sun and each of the eight planets of the Solar System is much smaller than this value. Therefore, in the majority of real cases, the triangular libration points are stable. On the other hand, the unstable character of the collinear libration points allows to define dynamical structures responsible for the transport of material to/from their neighbourhood.

The central part of the collinear libration points is associated with planar periodic orbits, revolving around them [1]. Initials conditions for such orbits, called planar Lyapunov orbits (PLO) can be found from the linearized equations by imposing that $y = z = 0$, $\dot{x} = \dot{z} = 0$ at $t = 0$. Integrating the initial state in the non-linear model, i.e., Eqs. (2) and adding the constraint of periodicity by means of a single-shooting algorithm we can identify these periodic orbits and eventually a *family* of PLO. In Fig. 4 an example of PLO families around L_1 and L_2 for the Earth-Moon systems is displayed.

3.2 Invariant manifolds of periodic orbits

The analysis of eigenvectors associated to matrix **A** (Eq. (5)) permits to define stable and unstable subspaces associated to equilibrium points in the linearized space. In particular, the set of all the eigenvectors with positive real part define the stable subspace, while eigenvectors with negative real part define the unstable subspace. By means of the centre manifold theorem [6, 7] we can prove the

[1] The central part is actually related to non-planar orbit as well. Among them, *vertical Lyapunov orbits*, *Halo orbits* and the quasi-periodic *Lissajous* trajectories.

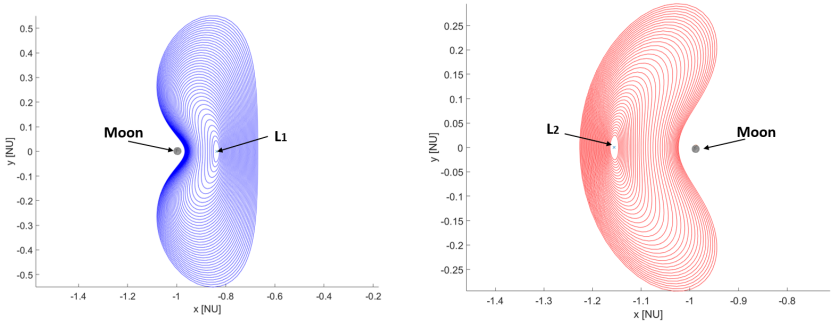

(a) PLOs familiy around L_1 (b) PLOs familiy around L_2

Figure 4: PLO families around L_1 and L_2 for the Earth-Moon system (Moon not to scale). Notice that PLOs around L_2 are bigger than orbits around L_1.

existence of invariant manifolds (IMs) associated to equilibrium points: these objects are the counterpart of subspaces when using the non-linear model and they are tangent to relative subspace in the equilibrium point. Should P_3 belong to the six-dimensional stable (or unstable) manifold related to the equilibrium point P_i $(i = 1, 2, 3)$ it will asymptotically tend towards the equilibrium point itself for $t \to +\infty$ $(t \to -\infty)$.

These structures can be defined also for periodic orbits (such as PLOs) of the collinear points. Both stable and unstable IMs for periodic orbits are characterized by two *branches*. Projections of these object into the bi-dimensional space defined by the x and y coordinates are represented in Fig. 5 for the Earth-Moon system. We often refer to these projections as *manifold tubes*. Stable IMs converge to the corresponding PLO for $t \to +\infty$, while unstable IMs converge to the corresponding PLO for $t \to -\infty$.

3.3 Transit orbits

A key feature of IMs is that they act as separatrices for the flow through the equilibrium region, i.e., they separate two distinct types of motion: *transit orbits*, which move inside the manifold tubes and *non-transit orbits* which are those outside the tubes. Moreover, only TOs can travel between the interior and the exterior region, thus controlling the transport of material to and from the L_2 bottleneck. As a consequence, for a given Jacobi constant J, all the TOs will pass inside the region defined by the PLO around L_2 with the same energy. In Fig. 6 examples of transit and non-transit orbits are provided for the Earth-Moon planar CR3BP.

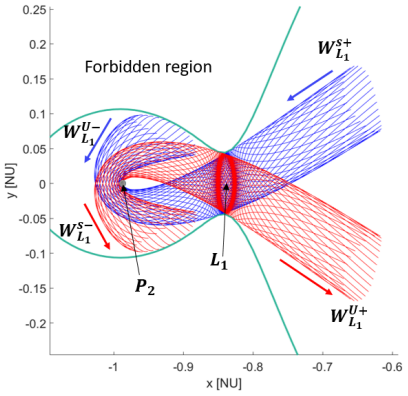

(a) IMs originating from PLO around Earth-Moon L_1. $J = 3.18067$, propagation time: 23.05 days

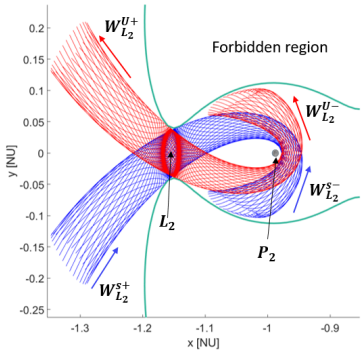

(b) IMs originating from PLO around Earth-Moon L_2. $J = 3.19238$, propagation time: 17.39 days

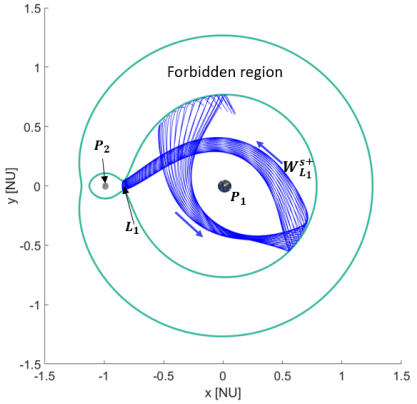

(c) Stable IM originating from PLO around Earth-Moon L_2. $J = 3.19238$, propagation time: 38.26 days

Figure 5: Different IMs morphologies originating from PLOs around L_1 and L_2 points of the Earth-Moon System. Exponents "+" and "-" for a given stable $W^S_{L_i}$ or unstable $W^U_{L_i}$ IM ($i = 1, 2$) represents the two different branches.

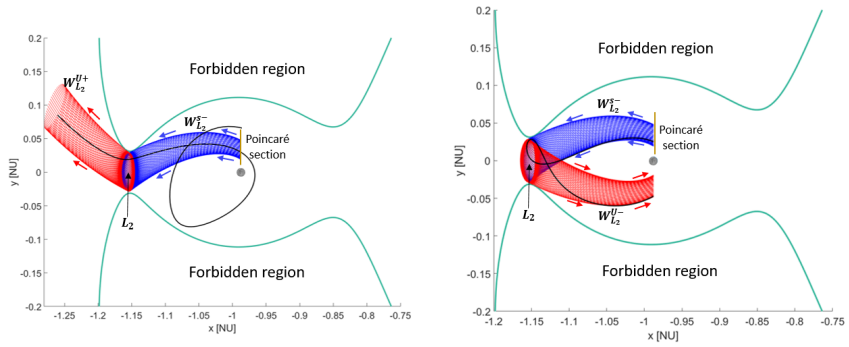

(a) Transit orbit

(b) Non-transit orbit

Figure 6: Examples of transit (left) and non-transit (right) orbits. Stable and unstable IMs of the PLO around L_2 are represented in blue and red respectively.

4 The indirect coupled circular-restricted three body problem

In the present work, the planar CR3BP is used to identify connections between consecutive moons of a planetary system, with the primaries being a planet and one of its moon and the third massless body is the spacecraft. This is done by means of the so called *coupled* CR3BP [9, 10] However, instead of using the CR3BP equations for the whole transfer (as done in the quoted papers), the two-body approximation is used in regions where the influence of the moon's gravity is negligible (*inter-moon space*). The boundary between the inter-moon space and the *intra-moon space* (where the CR3BP is used) is called *circle of influence* (CI). We define the radius of the circle of influence r_{CI} as the radius of the Laplace sphere multiplied by a convenient factor k:

$$r_{\text{CI}} = k r_0 \left(\frac{m}{M}\right) \tag{6}$$

being r_0 the radius of the moon, m its mass and M the mass of the planet. These concepts are clarified in Fig. 7 for a planetary system composed by a planet and three moons. The coordinate system adopted when describing the inter-moon dynamics is the planet-centred IRF; the value of k will be clarified later.

In order to perform the coupling, a coordinate change is applied from each SRF to the planet-centred IRF at the boundary between the inter-moon and intra-moon space, i.e., at the CI. This transformation requires a translation from the barycentre of the planet-moon system to the centre of the planet and a rotation about the z-axis by the angle between the x-axes of the SRF and the X-axis of the IRF. However, in this work we ignore the first translation being the centre of mass of the planet-moon system within a negligible distance from

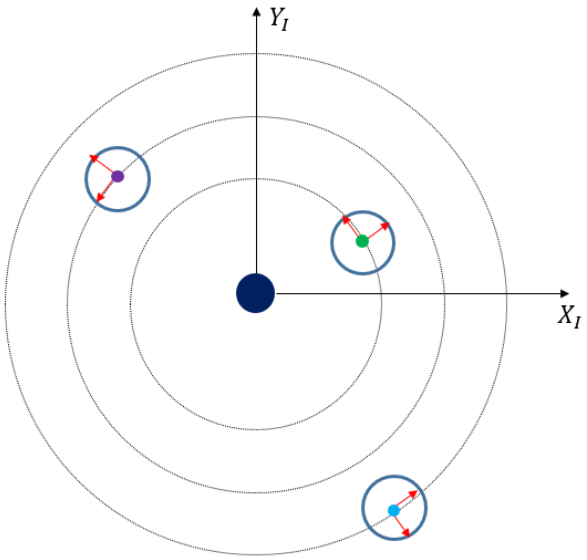

Figure 7: A planetary-system with three moons. The planet-centred IRF is represented in black, while the SRFs for each moon are represented in red (the x-axes are in the direction of the vector connecting the planet to the given moon). The intra-moon space is defined by the regions inside each CI (represented in blue), where the CR3BP is used. In the remaining region, defining the inter-moon space, the two-body approximation is adopted. Each moon is in a circular orbit around the planet.

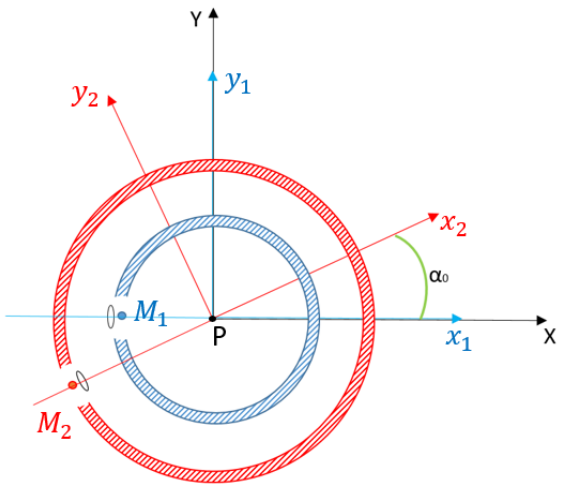

Figure 8: The coupled CR3BP for two consecutive moons M_1 and M_2 in circular motion around the planet P at constant angular velocity. The plot outlines the coupling at the time $t = 0$, with the x_1-axis aligned with the inertial X-axis. The angle α_0 between the two SRFs parametrises the model. For the sake of illustration, the forbidden region corresponding to the Jacobi constant value for two PLOs around P_1 or P_2 is represented for both the SRFs.

the centre of the planet in the majority of real cases (for example each planet-moon barycentre of the Galilean moons is three to six orders of magnitude smaller than the radius of Jupiter). The overall coupling between two moons depends on the relative angles swept by the x-axis of the SRFs with respect to the X-axis of the IRF. However, we choose to orient the IRF so that one of the two x-axis coincides with the inertial X-axis at $t = 0$: this allows to remove the dependence on one of the two angle. Therefore, the transformation has just one degree of freedom, represented by the relative angle α_0 between the two x-axes, as sketched in Fig. 8 for two consecutive moons of a planetary system. Moreover, since the angular velocities of the moons are constant, we can choose the angle α_0 at any fixed time to completely parametrise the model. We can use this parameter to map all the possible relative orientations between two moons in search for the optimal trajectory which links them. Taking advantage of the full integrability of the two-body model employed for the inter-moon connection, we can analytically solve for the best α_0 instead of scanning all the possible solutions associated with its values. In this work two methods are used to identify trajectories in the intra-moon space, i.e., by means of IMs and TOs.

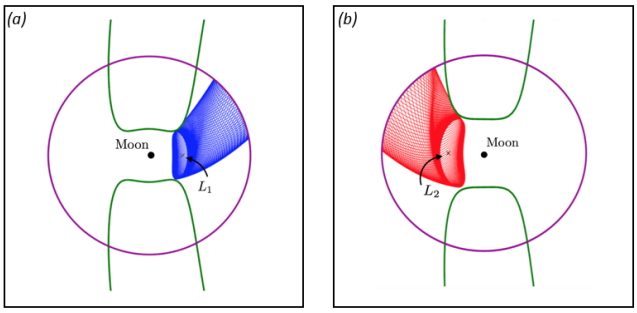

Figure 9: Stable and unstable IMs originating from a PLO around P_1 (left) and P_2 (right), integrated until the CI and used for the outward connection.

4.1 Integration of trajectories in the intra-moon space.

An outward connection between two consecutive moons (i.e., a link from the inner to the outer moon) by means of IMs is conceived as a trajectory leaving a PLO around P_2 of the inner moon through the unstable manifold and approaching a PLO around P_1 of the outer moon through the unstable manifold. Similarly, an inward connection is conceived as a trajectory leaving a PLO around P_1 of the outer moon through the unstable manifold and approaching a PLO around P_2 of the inner moon through the stable manifold. PLOs are varied according to a certain energy discretization, leading to a database to be used in the trajectory design. For each PLO of the database, the corresponding stable (or unstable) IM is propagated until intersection with the CI (see Fig. 9). The phase states collected on the CIs are transformed to the planet-centred IRF and considered as initial conditions for backward/forward integration.

In the case of the TOs, instead of leaving/approaching the PLO, the trajectory pass through it. For this reason, we select initial conditions for the TOs directly inside the region defined by each PLO of the database by means of a $n_X \times n_Y$ grid (see Fig. 10). Since each PLO is computed numerically as a set of points, an analytical representation of the PLO is needed to distinguish between points inside or outside the grid: this is accomplished by approximating the PLO through a parametric cubic spline. Only points inside the grid are selected as initial conditions. For a given position (x_0, y_0) and a value of the Jacobi constant J, the magnitude of the initial velocity is constrained by Eq. (3): Therefore, once selected an angle β (see Fig. 10) between the velocity direction and the positive x-axis, the remaining velocity components of the initial state $\dot{x}_0$ and $\dot{y}_0$ are given, being:

$$\begin{cases} \dot{x} = v\cos\beta \\ \dot{y} = v\sin\beta \end{cases} \tag{7}$$

where $\beta \in [0, 2\pi[$. We call n_β the number of directions in which the angular range $[0, 2\pi[$ is discretized. A given initial state for a TO is therefore a function of the position (x_0, y_0) on the grid, the Jacobi constant J and the angle β. Varying

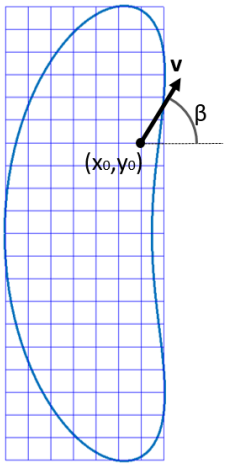

Figure 10: 8×21 grid around a PLO. Only points (x_0, y_0) inside the Lyapunov region are selected as initial conditions for trajectory computation. The velocity components $(\dot{x}_0, \dot{y_0})$ are selected through equation (7) for a given angle β.

the position on the grid and the remaining two parameters permits to define a set of initial states $(x_0, y_0, \dot{x}_0, \dot{y}_0)$ to be integrated by means of Eqs. 2 until intersection with the CI. Eventually, the phase states at the CI are converted from the SRF to the planet-centred IRF.

4.2 Motion in the inter-moon space

The two-body approximation in the planet-centred IRF substitutes the CR3BP when dealing with the spacecraft's dynamics beyond the CI, i.e., in the inter-moon space. The initial states on the CI expressed in the planet-centred IRF are used as initial conditions for backward/forward Keplerian orbit propagation. No matter the time direction, these Keplerian orbits are ellipses with a focus on the planet's centre. These ellipses are completely parametrised by the semi-major axis a, the eccentricity e, the argument of pericentre ω and supplemented by the true anomaly θ which parametrises the motion along the ellipse (in the planar approximation, the inclination and the right ascension of the ascending node are irrelevant). Since the two ellipses shares the same focus (this focus being the planet) it is easy to prove that the maximum number of intersections between them is two. The semi-major axis and the eccentricity provide the shape of the ellipse, and as such are fixed for a given state on the CI. On the contrary, the argument of pericentre depends only on the relative orientation between the x-axis with the XY-plane at the given time. In other words, a change $\Delta\alpha$ in the orientation of the SRF produces an equivalent change $\Delta\omega = \Delta\alpha$ of the argument of pericentre of the resulting ellipse.

The procedure to find possible intersections is now presented. For a choice

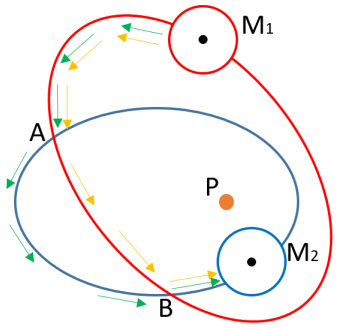

Figure 11: Two possible path (showed by means of orange and green arrows) from the CI of moon M_1 to the CI of moon M_2 through the intersections A and B. The two ellipses share the same focus represented by the planet P.

of two PLOs, one on each CR3BP, IMs and TOs are integrated with the method described in the previous section. For a choice of α_0 the phase states are collected on the two CIs and converted into Keplerian elements sets. Connections between moons are then sought by looking at the geometrical intersections between all the possible combinations of ellipses from the two CIs. If an intersection between two ellipses exist, the magnitude ΔV of the difference in velocity at the intersection point is the magnitude of the impulse to be applied by the propulsion system of the spacecraft to change from one orbit to another and eventually accomplish the task of connecting the two CR3BPs. If more than one intersection exist, two possible paths connecting the two moons are available and the ΔV at each intersection will be different. Figure 11 shows two ways to connect the CIs of two moons by means of the two paths provided by intersections A and B. This procedure should be repeated for every angle α_0 between 0 and 2π. Comparing all the possible combinations of ellipses, the initial conditions providing the minimum ΔV can be found. This may become time-consuming if the resolution taken to discretise the angle α_0, the individual PLO (or the related grid, in case of TOs) and the energy level of the Lyapunov family is narrow. However, a closer look allows to simplify the problem and, in turn, reduce the amount of computations. We start by writing the polar equation of the ellipse, providing the distance r of the spacecraft to the focus as a function of the true anomaly θ:

$$r = \frac{p}{1 + e\cos\theta} \tag{8}$$

being $p = a(1 - e^2)$ the *semilatus rectum* of the ellipse. At the intersection points A and B between two ellipses defined by the orbital sets (a_1, e_1, ω_1) and

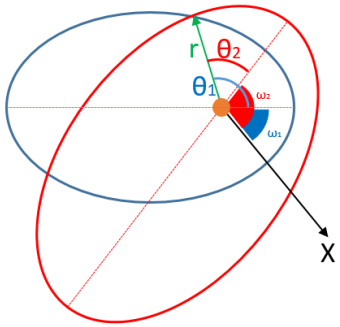

Figure 12: Intersection point between two ellipses sharing the same focus. The radius r is the same in this point, while the true anomalies θ_1 and θ_2 vary according with the two argument of perigee ω_1 and ω_2 (referred to the inertial X-axis).

(a_2, e_2, ω_2) (see Fig. 12), the orbit equations can be written as:

$$r = \frac{p_1}{1 + e_1 \cos\theta_1}, \tag{9a}$$

$$r = \frac{p_2}{1 + e_2 \cos\theta_2}. \tag{9b}$$

The angular displacement between the two apse lines is

$$\Delta\omega = \theta_2 - \theta_1, \tag{10}$$

hence

$$\cos(\theta_2) = \cos(\theta_1 + \Delta\omega) = \cos\theta_1 \cos\Delta\omega - \sin\theta_1 \sin\Delta\omega. \tag{11}$$

From Eqs. (9) and (11) it follows

$$p_1 - p_2 + \cos\theta_1 \left[p_1 e_2 \cos\Delta\omega - p_2 e_1\right] = \sin\theta_1 (p_1 e_2 \sin\Delta\omega) \tag{12}$$

or, in a more compact form

$$a + b\cos\theta_1 = c\sin\theta_1, \tag{13}$$

where we made the substitutions:

$$a = p_1 - p_2, \tag{14a}$$

$$b = p_1 e_2 \cos\Delta\omega - p_2 e_1, \tag{14b}$$

$$c = p_1 e_2 \sin\Delta\omega. \tag{14c}$$

Squaring both the members of Eq. (13) and rearranging yields:

$$\cos\theta_1 = \frac{-ab \pm |c|\sqrt{c^2 + b^2 - a^2}}{b^2 + c^2}. \tag{15}$$

Solutions exist and are real only if the discriminant is positive:

$$c^2 + b^2 - a^2 \geq 0, \tag{16}$$

where the equality

$$c^2 + b^2 - a^2 = 0, \tag{17}$$

corresponds to the tangency condition between the two ellipses. From (13):

$$\sin\theta_1 = \frac{a + b\cos\theta_1}{c}, \tag{18}$$

hence, the correct quadrant of the angle θ_1 can be found using (15) and (18). Once the two intersections are found, the radial and perpendicular components of the velocity are computed for each orbit:

$$v_{r,ij} = \frac{\mu}{h} e \sin\theta_{ij}, \tag{19a}$$

$$v_{\perp,ij} = \frac{\mu}{h}(1 + e\cos\theta_{ij}). \tag{19b}$$

where the first index i represents the orbit ($i = 1, 2$) and the second index j represents the intersection ($j = 1, 2$). Hence, we can write the velocity at each intersection as:

$$\mathbf{v_{ij}} = v_{r,ij}\hat{\mathbf{u}}_{r,ij} + v_{\perp ij}\hat{\mathbf{u}}_{\perp,ij}, \tag{20}$$

being $\hat{\mathbf{u}}_{r,ij}$ and $\hat{\mathbf{u}}_{\perp,\mathbf{ij}}$ the unit vectors related to the radial and perpendicular velocity components $v_{r,ij}$ and $v_{\perp,ij}$. Therefore the $\Delta\mathbf{v}_j$ for each intersection j will be:

$$\Delta\mathbf{v}_j = \mathbf{v}_{2j} - \mathbf{v}_{1j}. \tag{21}$$

The condition on the discriminant (Eq. (16)) translates into a condition for $\Delta\omega$ to be satisfied, i.e. the two ellipses intersect only in a limited range of values for $\Delta\omega$:

$$\tau \leq \Delta\omega \leq 2\pi - \tau, \tag{22}$$

with $\tau \in [0, 2\pi[$. The value of τ depends only on the shape of the two ellipses and can be explicitly calculated in terms of a_i and e_i ($i = 1, 2$) from the the tangency condition, given by Eq. 17. For $\tau > 0$ the domain of intersections is limited by the conditions at which the ellipses are mutually tangent (Fig. 13), i.e., $\Delta\omega = \tau$ and $\Delta\omega = 2\pi - \tau$. On the other hand, if $\tau = 0$ no tangency condition exists and the two ellipses always have two intersections, regardless their relative orientation. In theory, one should vary $\Delta\omega$ for each pair of ellipses and then choose the value that minimizes $\Delta V = \|\Delta\mathbf{v}\|$ in one of the two intersections. Actually, as our intuition suggests, the minimum ΔV values corresponds to the tangency configuration. In order to prove it, we analysed the value of ΔV as a function of $\Delta\omega$ for several pairs of ellipses, varying the semi-major axis and the eccentricity. For each pair, the value of τ has been determined and, by varying $\Delta\omega$ between τ and $2\pi - \tau$ the value of ΔV has been computed at every intersection. The results show that if $\tau > 0$, the ΔV has two minima for

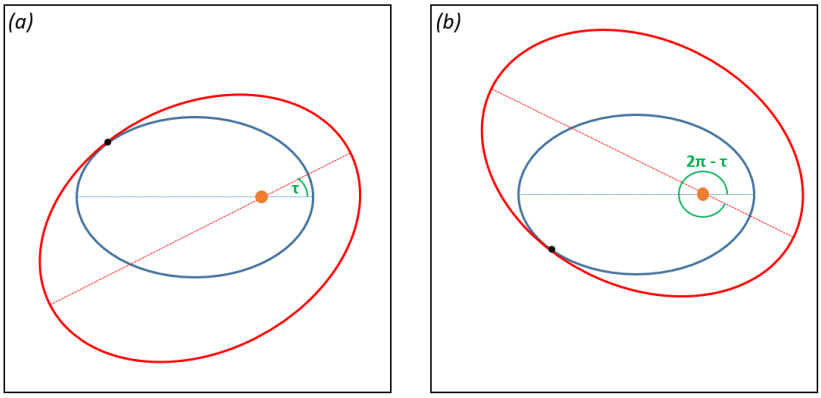

Figure 13: Relative angular displacement $\Delta\omega$ between the arguments of perigee of two ellipses when they are mutually tangent. The configuration is symmetrical and the two ellipses are tangent for $\Delta\omega = \tau$ (left) or $\Delta\omega = 2\pi - \tau$ (right).

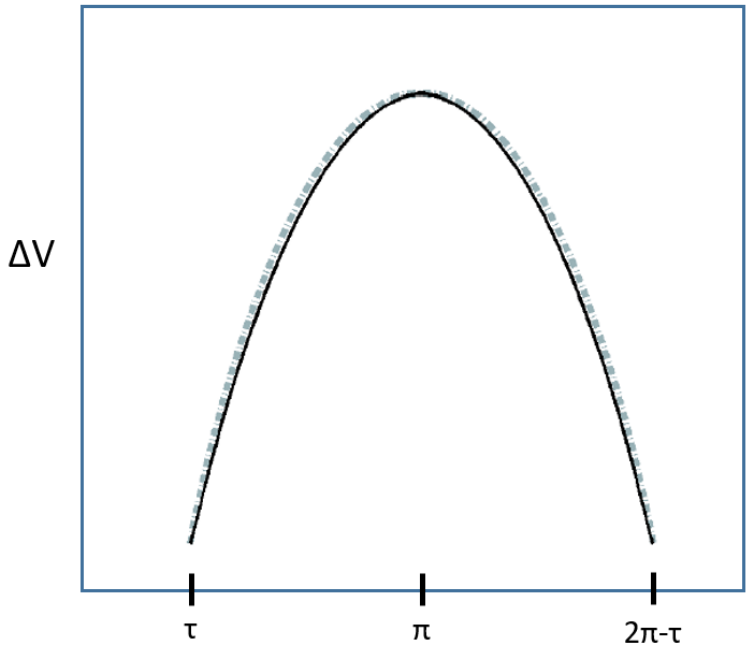

Figure 14: ΔV at the intersections between two ellipses versus their relative orientation $\Delta\omega$. The two different curves (solid and dashed) stand for the Δv at the two different intersection. The minima correspond to the tangency configuration while the maximum is for $\Delta\omega = \pi$.

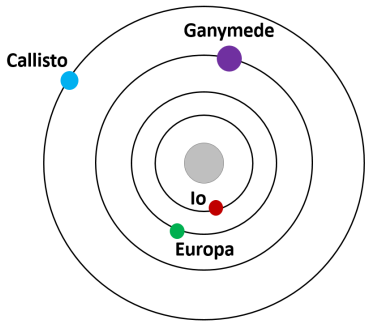

Figure 15: The orbits of the Galilean moons (the radii of Jupiter and the moons are not to scale)

$\Delta\omega = \tau$ and $\Delta\omega = 2\pi - \tau$, i.e., when the ellipses are mutually tangent. On the other hand, the ΔV is maximum when $\Delta\omega = \pi$, that is when the two apse lines are opposite (see Fig. 14). This behaviour always occurs at least when the eccentricities are smaller than 0.2. In our case, since the ellipses studied are an extension of the motion originating in the vicinity of the libration points, their path in the IRF must inherit the behaviour of the corresponding equilibrium points, which move in circular orbits around the planet. Therefore, these orbits are expected to have low eccentricities and this guarantee the applicability of the intersection pattern shown in Fig. 14.

4.3 Application to a transfer from Europa to Ganymede and viceversa

In this section we present an application of the method described to the case of a transfer between two consecutive Galilean moons, Europa and Ganymede. The orbits of the four Galilean moons are represented to scale in Fig. 15. Relevant orbital parameters are listed in Table 1. Connections are sought by means of IMs and TOs in the inter-moon space. In the case of IMs, the transfer connects two PLOs, one around L_2 of Jupiter-Europa and the other around L_1 of Jupiter-Ganymede. On the other hand, when dealing with TOs, the trajectory links one point inside a PLO around L_2 of Jupiter-Europa and one inside a PLO around L_1 of Jupiter-Ganymede. PLOs are taken from two databases of 95 orbits (see Fig. 16), each discretized in 99 points. Jacobi constant for PLOs around P_2 ranges from 3.001631769881 to 3.003593748544, while for PLOs around Ganymede P_1 the range is from 3.005357382121 to 3.007543590510 (sorted from 1 to 95 in increasing energy order, i.e., with decreasing Jacobi constant). The best coupling between the two CR3BPs is the one that minimizes the ΔV at the intersection point between the two ellipses at their tangent configuration in the inter-moon space.

When IMs trajectories are used in the intra-moon space, the absolute minimum is $\Delta V_{\text{MIN}} = 0.8814\,\text{km}\,\text{s}^{-1}$ in both directions Europa-to-Ganymede and

Moon	Orbital radius [10^5 Km]	Orbital Period [days]	Mass ratio [10^{-4}]
Io	4.2180	1.8	0.470542991630
Europa	6.7110	3.6	0.252865845179
Ganymede	10.7040	7.2	0.780632933465
Callisto	18.8270	16.7	0.566808592975

Table 1: The second and the the third columns represent respectively the radii and the orbital periods of the Galilean moons. The fourth column lists the mass ratios $m_i/(m_i + m_J)$, being m_i the mass of the moon and $m_J = 0.189\,813 \times 10^{28}$ kg the mass of Jupiter.

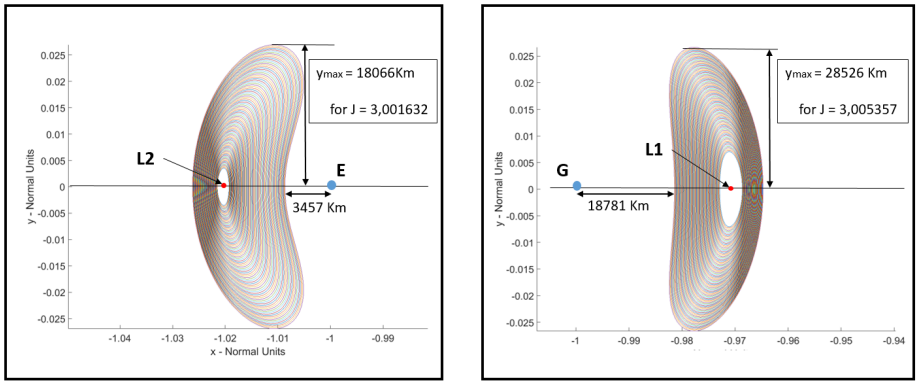

Figure 16: The database of PLOs around L_2 in the Jupiter-Europa CR3BP (left) and around L_1 in the Jupiter-Ganymede CR3BP (right) shown in their respective SRF. The maximum amplitude in the y direction of the largest PLO and its minimum distance to the moon are displayed.

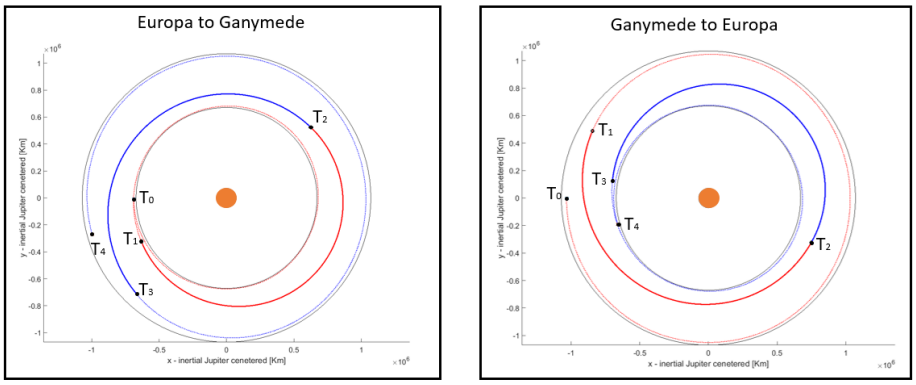

Figure 17: Transfer from Europa to Ganymede (left) and viceversa (right) as viewed from the Jupiter-centred IRF with the IMs method inside the CI. The trajectory is represented with a dashed line as long as the spacecraft is inside the CI while it is a continuous line on the Keplerian ellipses.

Ganymede-to-Europa. It is obtained for the PLO number 95 in both the databases, corresponding to the highest energies of the database. The minimum-cost trajectories are shown in Fig. 17.

In case of TOs, the initial conditions required for integration in the intra-moon space are selected inside the PLOs of the database, This is done by means of a grid of points, as described in Sect. 4.1. Grids are computed with the following criteria:

1. The border of the grid is tangent to the PLO.
2. The distance between two consecutive points on the grid is constant in both the directions x and y.

As a consequence of the second criterion above mentioned, n_Y will vary according to the y-amplitude of the PLO. Each grid is then completely parametrized by n_X and n_β. For this application, we choose a gird discretization with $n_X = 5$. To select the velocity angles β, discrete values in the range $R^- = [\pi/2, 3\pi/2]$ are chosen if the TOs are moving towards L_2 forward in time; on the other hand if the TOs are moving towards L_1 forward in time, values in the range $R^+ = [3\pi/2, \pi/2]$ are selected. Since a TO crosses the equilibrium regions flowing inside the spatial bi-dimensional projection of the same-energy manifold tube, the right angular range can be inferred looking at the motion provided by the latter. Analysing the manifold tubes for a transfer Europa-to-Ganymede, we deduce the range R^- must be chosen (see Fig. 18). For this application we select $n_\beta = 3$ with the velocity angles $\beta_1 = 3\pi/4$, $\beta_2 = \pi$ and $\beta_3 = 5\pi/4$. Similarly, the reverse transfer Ganymede-to-Europa requires the range R^+ and we select $\beta_4 = 3\pi/4$, $\beta_5 = \pi$ and $\beta_6 = 5\pi/4$. The minimum ΔV in this case is $\Delta V_{\text{MIN}} = 0.5145\,\text{km}\,\text{s}^{-1}$ in both directions and, again, it is associated with

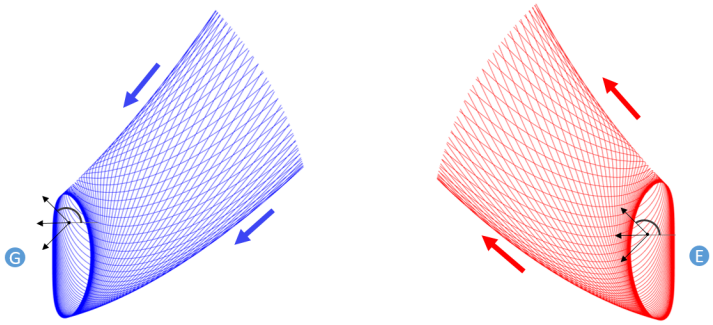

(a) Velocity directions for a grid point inside a PLO around Europa

(b) Velocity directions for a grid point inside a PLO around Ganymede

Figure 18: Selected velocity directions for the transfer Europa-to-Ganymede using TOs, i.e., $\beta_1 = 3\pi/4$, $\beta_2 = \pi$, $\beta_3 = 5\pi/4$ (represented by three black arrows). These values are the same for all the grid points inside the PLOs around Europa (a) and Ganymede (b).

the highest energies of the two databases. A plot with the transfers in the Jupiter-centred IRF is reported in Fig. 19.

In conclusion, the transfer performed by means of TOs is clearly faster than the corresponding coupling with IMs (2.78 days versus 12.38 days) as well as cheaper in terms of ΔV ($514.5\,\mathrm{m\,s^{-1}}$ versus $881.4\,\mathrm{m\,s^{-1}}$). In particular, TOs do not spend any time in asymptotic motion around the PLO. The shorter time of flight provided by TOs makes them more feasible for a real mission. In fact, the intense particle radiation due to the Jovian magnetosphere, which extend almost to the orbit of Ganymede, may represent a serious obstacle to the practical implementation of trajectories that spends days in the intra-moon space.

5 Galilean Moons tour

Recursive application of the indirect coupled CR3BP explained in the previous section can be employed to design a *tour* of a planetary system with n moons. In this case we take into account the Galilean moons Europa, Ganymede and Callisto. Io has been excluded because of the strong influence from Jupiter's magnetosphere (more intense with respect to the other moons).

Transit orbits are chosen as a means of transport for the tour; the reason of this choice is the shorter time of flight provided with respect to IMs trajectories. Moreover, the tour must be closed, i.e., starting from a state on Europa, the trajectory must cross the vicinity of all the selected moons and then come back to the same initial state on Europa. The following constraints are chosen to recursively apply the indirect coupled CR3BP:

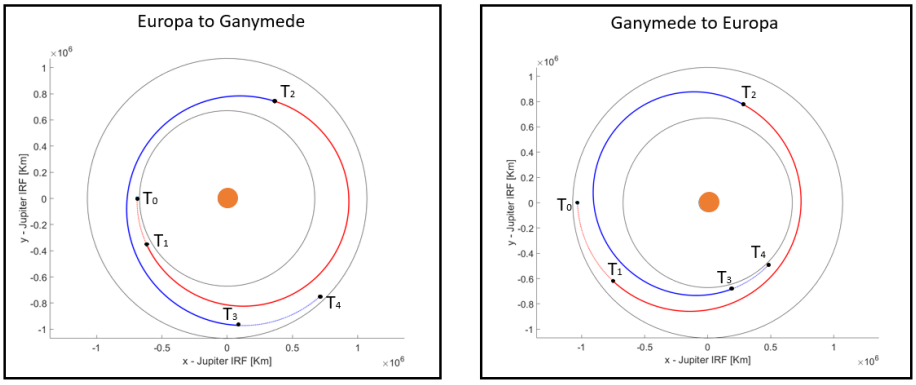

Figure 19: Transfer from Europa to Ganymede (left) and viceversa (right) as viewed from the Jupiter-centred IRF with the TOs method inside the CI. The trajectory is represented with a dashed line as long as the spacecraft is inside the CI while it is a continuous line on the Keplerian ellipses.

- On Europa and Callisto the trajectory must turn around the respective moon by an angle of π (see Fig. 20(a)(c)).
- On Ganymede, the trajectory must turn around the moon by an angle of 2π (see Fig. 20(b)).
- The minimum approach distance from the moon surface must be grater than 50 km.

With *outward journey* we refer to the trajectory from Europa to Callisto; viceversa the *inward journey* is the trajectory from Callisto to Europa. Transit orbits will be generated using the method described in the previous section, i.e., by means of grids built around a set of PLO associated to specific Lagrangian points of each Jupiter-moon system. Setting $t = 0$ on each grid initial condition, we talk about *time-backward* and *time-forward* TO branches (TBB and TFB respectively): the former refer to the branch integrated backward in time, the latter to the branch integrated forward in time. Grids are generated according with the following (refer to figure 20) criteria.

- For Jupiter-Europa, grids are built by means of PLOs around L_2. TFBs point towards Ganymede.
- For Jupiter-Ganymede (outward journey), grids are built by means of PLOs around L_1. The spacecraft is approaching the CI from Europa through the TBB and is pointing towards Callisto passing through the TFB.
- For Jupiter-Callisto, PLOs around Jupiter-Callisto L_1 will be used. The spacecraft is coming from Ganymede through the TBB.

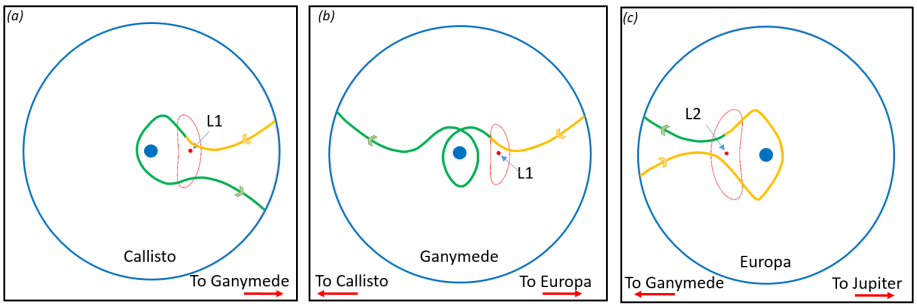

Figure 20: Transit morphologies. Europa is represented in figure (c) with Jupiter towards the right. Callisto (the outer moon), is represented in figure (a). Time-forward and time-backward TOs are represented in green and orange respectively. CIs are represented in blue and, for the sake of clarity, the PLO with the same energy of the corresponding TO is plotted in red.

- For Jupiter-Ganymede (inward journey), grids are built by means of PLOs around L_2. The spacecraft is approaching the CI from Callisto through the TBB and is pointing towards Europa passing through the TFB.

Recursively applying the coupled CR3BP at each connection (Europa to Ganymede, Ganymede to Callisto, Callisto to Ganymede and Ganymede to Europa) with a similar method as the one described in the previous section, a set of initial conditions that provide close tours can be found. Since, in general, the minimum approach distance to the moon is high for the resulting TOs, we decided to select the tour that minimizes this parameter. This tour is characterized by:

$$\Delta V = 1.067 + 1.142 + 1.156 + 1.229 = 4.59\,\mathrm{km\,s^{-1}}, \tag{23}$$

$$\mathrm{TOF} = 4.355 + 15.343 + 18.681 + 10.723 = 49.102\,\mathrm{days}, \tag{24}$$

The trajectories of this tour in the intra-moon space are displayed in Fig. 21.

5.1 Rephasing

Each of the four coupled CR3BPs that define the tour requires a specific angular displacement $\Delta\alpha_{ij}$ between the two moons i and j ($i, j = 1, 2, 3$, $i \neq j$, 1: Europa, 2: Ganymede, 3: Callisto) when the spacecraft leaves the initial condition from moon i. This value depends on the tangency configuration between the corresponding Keplerian ellipses as well as on the time the spacecraft spends inside each CI. We define T_{ij} the time of flight required from the spacecraft to go from the initial condition on the moon i to the initial condition on the moon j. Once fixed an initial angular position α_{01} of Europa at the beginning of the outward journey, i.e., at $t = 0$ (where t is the cumulative time of the tour), the initial angular position on Ganymede must be

$$\alpha_{02} = \alpha_{01} + \Delta\alpha_{12} - \omega_2 T_{12}, \tag{25}$$

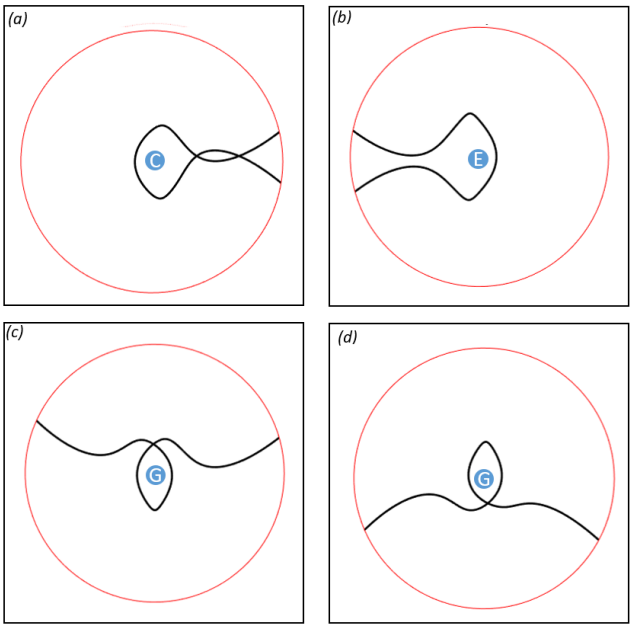

Figure 21: The resulting trajectories of the selected minimum-approaching-distance tour in the intra-moon space for Europa (top-right), Callisto (top-left), Ganymede outgoing (bottom-left) and Ganymede ingoing (bottom-right).

where ω_i is the angular velocity of the i^{th} moon. Similarly, the angular position required by Callisto at $t = 0$ must be

$$\alpha_{03} = \alpha_{01} + \Delta\alpha_{12} + \Delta\alpha_{23} - \omega_3(T_{12} + T_{23}). \tag{26}$$

When the spacecraft reaches Callisto and therefore ends the outward journey, the coupled CR3BP with Ganymede to start the inward journey requires a specific angular displacement $\Delta\alpha_{32}$ between these two moons. Therefore, the requisite on the initial angular position at $t = 0$ for Ganymede would now be

$$\alpha'_{02} = \alpha_{01} + \Delta\alpha_{12} + \Delta\alpha_{23} + \Delta\alpha_{32} - \omega_2(T_{12} + T_{23} + T_{32}), \tag{27}$$

which, in general, is different from the angle in Eq. (25). Therefore, it is necessary to "pause" the tour once the spacecraft leaves Callisto; in other words, in order for the tour to exist, we should find a suitable parking (or *rephasing*) orbit where the spacecraft can temporary wait until Callisto and Ganymede are in the correct relative angular position $\Delta\alpha_{32}$. It can be easily proved that the necessary rephasing time is

$$T_{\text{REPH}} = \frac{\Delta\alpha'_{02} - \Delta\alpha_{02}}{\omega_2 - \omega_2} + n\frac{2\pi}{\omega_3 - \omega_2} \tag{28}$$

$$= T^* + nT_{\text{SYN}},\ n \in \mathbb{N}. \tag{29}$$

The first therm T^* of Eq. (28) is a constant and it depends only on the difference between $\Delta\alpha'_{02}$ and $\Delta\alpha_{02}$, which is a parameter of the tour; the second term is a multiple of the synodic period, therefore it is independent from the tour.

For example, in the case of Callisto, the required rephasing time is $T^3_{\text{REPH}}(n) = 2.68 + n15.21$. For a given value of n. The following algorithm has been created to find suitable rephasing orbits.

1. We select a set of points P on the TO in Callisto (Fig. 21(a)), such that their distance from the centre of the moon is below a given value.

2. For each of these points $\mathbf{r_i}$ we consider the corresponding velocity vector $\mathbf{v_i}$ of the TO. The flight path angle γ_i is given by $\cos\gamma_i = \dfrac{\mathbf{r_i} \cdot \mathbf{v_i}}{r_i v_i}$, being r_i and v_i the magnitudes of $\mathbf{r_i}$ and $\mathbf{v_i}$. A new set of velocity directions is computed varying the flight path angle in a given range $[\gamma_i - \Delta_\gamma, \gamma_i + \Delta_\gamma]$, being $\Delta_\gamma > 0$, for a given discretization. We call $\mathbf{v}_{ij}$ the j^{th} direction of the point $\mathbf{r_i}$

3. In turn, we let the magnitude of each velocity vector $\mathbf{v}_{ij}$ varying in a given range $[\mathbf{v_{ij}} - \Delta_v, \mathbf{v_{ij}} + \Delta_v]$, being $\Delta_v > 0$. We call $\mathbf{v}_{ijk}$ the k^{th} magnitude of the j^th velocity direction of the point $\mathbf{r_i} \in P$.

4. Each state $\{\mathbf{r_i}, \mathbf{v_{ijk}}\}$ is integrated for three revolutions around the moon. ΔV^1_{ijk} is the required difference in velocity to change the state from $\{\mathbf{r_i}, \mathbf{v_i}\}$ to $\{\mathbf{r_i}, \mathbf{v_{ijk}}\}$. If the trajectory remains inside the P_2 region, the distance δ (see Fig. 22) is evaluated after each revolution.

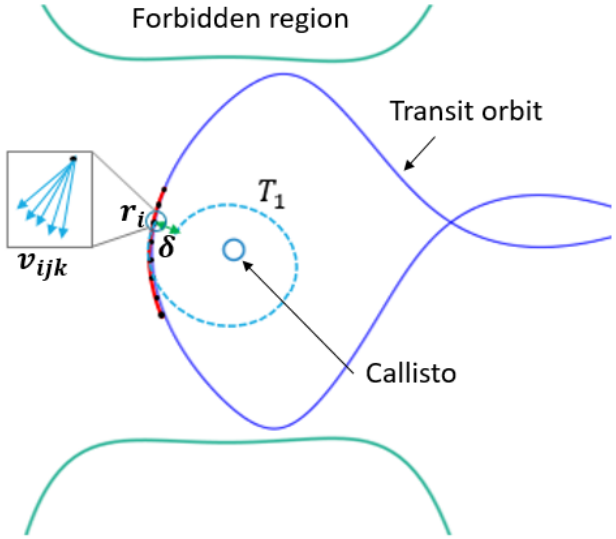

Figure 22: δ is the distance between $\mathbf{r_i}$ and the end point of the trajectory resulting by integration of the state $\{\mathbf{r_i}, \mathbf{v_{ijk}}\}$ after each revolution around the moon. T_1 is the period after one revolution.

5. If $\delta < 10^{-3}$ for all the three revolutions, we consider the orbit as stable and we store the corresponding state $\{\mathbf{r_i}, \mathbf{v_{ijk}}\}$ in a database. Moreover, we evaluate the time of flight T_1 to complete the first revolution. Since δ is very small, T_1 is an approximation of the time required to complete every complete revolution around the moon.

6. The *time performance parameter* is then defined as

$$\eta = \begin{cases} \mod\left(\frac{T_{\text{REPH}}(n)}{T_1}\right), \text{ if } \mod\left(\frac{T_{\text{REPH}}(n)}{T_1}\right) < 0.5, \\ 1 - \mod\left(\frac{T_{\text{REPH}}(n)}{T_1}\right), \text{ if } \mod\left(\frac{T_{\text{REPH}}(n)}{T_1}\right) > 0.5, \end{cases} \tag{30}$$

   When $\eta = 0$, $T_{\text{REPH}}(n)$ is a multiple of T_1. Therefore, values of η close to 0 identify more suitable stable rephasing orbits.

7. We select a range $[\eta^-, \eta^+]$. In this case we chose $\eta^- = \eta^+ = 0.1$. Each state $\{\mathbf{r_i}, \mathbf{v_{ijk}}\}$ in this range is propagated for m revolutions such that

$$T_{\text{REPH}} - \sum_{n=1}^{m} T_n \approx T_1. \tag{31}$$

   In other words, the states are propagated until approximately one more revolution is needed to reach the required rephasing time.

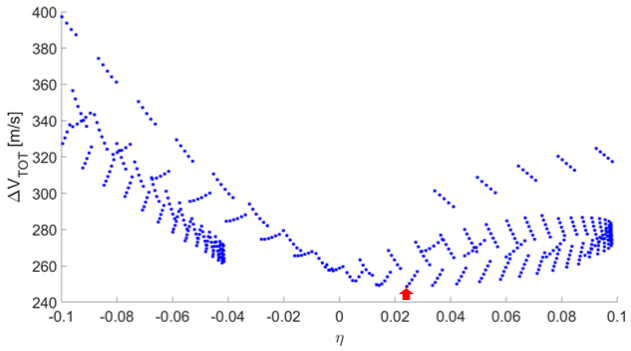

Figure 23

8. The last revolution is stopped after half-turn. We call T_f the cumulative time of flight required for the integration from the initial state $\{\mathbf{r_i}, \mathbf{v_{ijk}}\}$ until this half-turn. At this point a single-shooting algorithm with control on the velocity is used to target the initial position $\mathbf{r_i}$ with a constraint on the time of flight:
$$\text{TOF} = T_{\text{REPH}} - T_f. \tag{32}$$
ΔV^2_{ijk} is the required magnitude of the difference in velocity to target $\mathbf{r_i}$.

9. Eventually we evaluate the ΔV^3_{ijk} to re-insert the spacecraft in the original TO.

10. A plot of the total $\Delta V^{\text{REPH}}_{ijk} = \Delta V^1_{ijk} + \Delta V^2_{ijk} + \Delta V^3_{ijk}$ for every state $\{\mathbf{r_i}, \mathbf{v_{ijk}}\}$ within the range $[\eta^-, \eta^+]$ is represented in Fig. 23 for the rephasing around Callisto. The minimum is
$$\Delta V^{\text{REPH}}_{\text{min}} = 124 + 8 + 116 = 248\,\text{m}\,\text{s}^{-1}. \tag{33}$$

A plot of the resulting trajectory required for the rephasing on Callisto is showed in Fig. 24a. The same procedure is applied around Ganymede. In this case, the required rephasing time is $T^2_{\text{REPH}} = 5.65 + n7.08$ days where, again, we use $n = 1$. In this case, the minimum ΔV is
$$\Delta V^{\text{REPH}}_{\text{min}} = 150 + 29 + 133 = 312\,\text{m}\,\text{s}^{-1}, \tag{34}$$
and the corresponding rephasing trajectory is showed in Fig. 24b.

6 Conclusions

In conclusion, we presented an efficient method to find low-energy connections between moons of a planetary system. In the case of Jupiter's moons Europa,

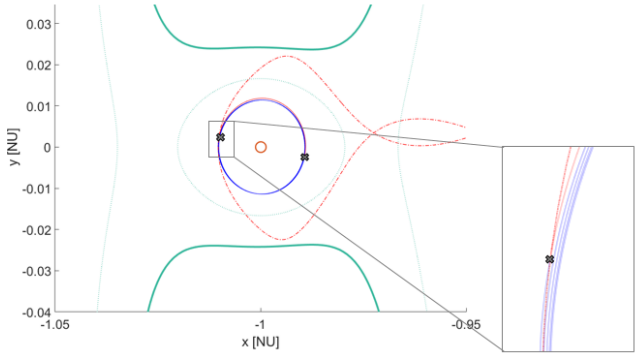

(a) Rephasing trajectory around Callisto

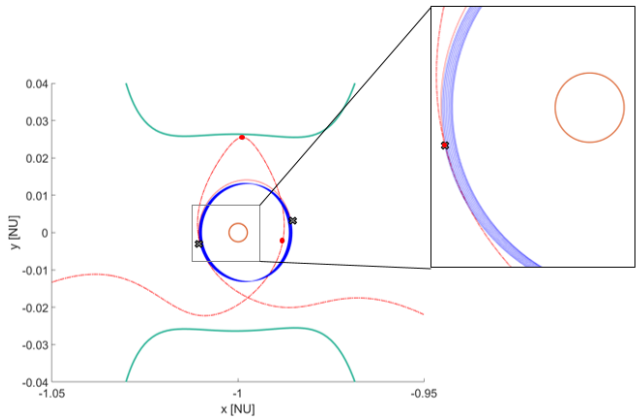

(b) Rephasing trajectory around Ganymede

Figure 24: Plot of the rephasing trajectories required for Europa (top) and Ganymede (bottom). Each "x" represents the position in which a ΔV is applied.

Ganymede and Callisto the total ΔV is on the order of $4\,\mathrm{km\,s^{-1}}$ plus $560\,\mathrm{m\,s^{-1}}$ requested for the rephasing. The first value is in agreement with previous studies [5] and substantially lower than the corresponding total ΔV expected for a Hohmann transfer, i.e., $10.88\,\mathrm{km\,s^{-1}}$. On the other hand, the total time of flight is about 77 days including the rephasing, which is more feasible than other studies involving multiple flybys [11] (in the quoted paper the time of flight to perform a tour of the four Galilean Moons is about 4 years). Since the ΔV in each of the four section is around $1\,\mathrm{km\,s^{-1}}$, low-thrust engines are more advisable to perform the manoeuvres. Conversion of the impulsive ΔVs into low-thrust arcs is currently under development.

References

[1] V. Szebehely, *Theory of orbit: The restricted problem of three Bodies*. Elsevier, 2012.

[2] G. Gómez and J. M. Mondelo, "The dynamics around the collinear equilibrium points of the rtbp," *Physica D: Nonlinear Phenomena*, vol. 157, no. 4, pp. 283–321, 2001.

[3] G. Gómez, *Dynamics and Mission Design Near Libration Points, Vol I: Fundamentals: the Case of Collinear Libration Points*, vol. 1. World Scientific, 2001.

[4] G. Gómez, À. Jorba, C. Simó, and J. Masdemont, *Dynamics and Mission Design Near Libration Points: Volume III: Advanced Methods for Collinear Points*, vol. 4. World Scientific, 2001.

[5] G. Gómez, W. Koon, M. Lo, J. Marsden, J. Masdemont, and S. Ross, "Connecting orbits and invariant manifolds in the spatial restricted three-body problem," *Nonlinearity*, vol. 17, no. 5, p. 1571, 2004.

[6] L. Perko, *Differential equations and dynamical systems*, vol. 7. Springer Science & Business Media, 2013.

[7] T. S. Parker and L. Chua, *Practical numerical algorithms for chaotic systems*. Springer Science & Business Media, 2012.

[8] F. R. Moulton, *An introduction to celestial mechanics*. Courier Corporation, 2012.

[9] R. Castelli, "Regions of prevalence in the coupled restricted three-body problems approximation," *Communications in Nonlinear Science and Numerical Simulation*, vol. 17, no. 2, pp. 804–816, 2012.

[10] W. S. Koon, M. W. Lo, J. E. Marsden, and S. D. Ross, "Dynamical systems, the three-body problem and space mission design," *Free online Copy: Marsden Books*, 2008.

[11] S. D. Ross, W. S. Koon, M. W. Lo, and J. E. Marsden, *Design of a multi-moon orbiter*. No. 114, American Astronautical Society, 2003.